30.0 MICROSTRUCTURAL EVOLUTION OF METALLIC ALLOYS DURING RAPID SOLIDIFICATION (LEVERAGED)

Chloe Johnson (CSM)
Faculty: Amy Clarke (CSM)
Other Participants: Yaofeng Guo (CSM), Joe McKeown (Lawrence Livermore National Laboratory)
Industrial Mentor: Los Alamos National Laboratory, Boeing

30.1 Project Overview and Industrial Relevance

Understanding the relationship between processing, microstructure, and final performance of a metallic alloy is a fundamental goal of materials science. This begins with understanding the as-solidified microstructure of a metallic alloy, as this can greatly impact subsequent solid-state microstructural evolution and the final microstructure. While conventional solidification techniques have been extensively studied, far from equilibrium processes that involve rapid solidification (e.g. additive manufacturing, AM) are not entirely understood. Processes like AM result in unique grain morphologies and metastable phases that can change the expected final properties of a metallic component. Because of this, it is important to understand the mechanisms controlling microstructural development during far from equilibrium processing to help predict and optimize performance.

Although rapid solidification studies have been performed on some aluminum alloys, most have involved post mortem characterization of microstructures. Only limited in-situ studies have been performed to date to observe rapid solidification of a few alloy systems [30.1-30.4]. This study proposes to use in-situ imaging techniques to understand microstructural development during rapid solidification of binary aluminum alloys (Al-Cu, Al-Ag, and Al-Ge). This will be coupled with ex-situ analyses to capture a large range of compositions and solidification conditions. Aluminum alloy powders with ceramic inoculants will also be imaged during processing for the first time. Investigating the effect of rapid solidification conditions on microstructural development will provide new understanding about emerging technologies like AM.

30.2 Previous Work

In-situ rapid solidification studies have been performed on Al-Cu and Al-Si alloys using the Dynamic Transmission Electron Microscope (DTEM) at Lawrence Livermore National Laboratory (LLNL) [30.1-30.2]. This technique images the evolution of the melt-pool during rapid solidification, capturing the growth of microstructural features and allowing for the determination of solidification velocities as features develop. This technique has been used to image Al-Ge, mainly to verify metastable phase diagrams proposed by Laoui and Kaufman, as shown in **Figure 30.1** [30.4], and to study faceting. The work of Laoui and Kaufman suggests that at compositions just below the solubility limit of the M (monoclinic) phase (i.e. below 50.5 at. % Ge), the M phase is the primary phase, given sufficient undercooling, while above this limit the M phase may form and re-melt in the liquid before the formation of the stable β phase. To try to capture this phenomenon, initial DTEM experiments were performed by our group across a wide variety of compositions (targeted 33-53 at. % Ge). The dynamic data resulting from these experiments captured some growth of M phase dendrites in the lowest composition (targeted 33 at. % Ge), and post mortem analyses showed that M + α eutectic developed between the M phase dendrites (**Figure 30.1**). Higher Ge content samples (measured to be 58 at. % Ge or higher) revealed the growth of Ge-rich, faceted β phase crystals; post-mortem microscopy showed a variety of eutectics (**Figure 30.1**), as well as some α phase dendrites surrounding β phase crystals. An initial study done by our group focused on identifying the phases in the two samples lowest in Ge (targeted to be 33 and 40 at. % Ge), as well as identifying the crystal structure of the M phase. These targeted compositions were measured to be 46 and 58 at. % Ge, rather than the targeted 33 and 40 at. % Ge. The M phase crystal structure was successfully determined using the 46 at. % sample, and the various eutectics in both of these samples were found to be M + α eutectic. This offset in composition, however, led to a need for more experimentation to obtain results closer to the 50.5 at. % Ge line, especially on the Ge-rich side. Also, the dynamic data for the samples above 50.5 at. % Ge needed further experimentation, as the first round of results did not capture the re-melting of the M phase in the liquid. Due to these issues, experiments in this area are ongoing.

Previous directional solidification studies performed by our group included Al-Ag alloys; this system was selected due to its tendency to exhibit significant solute segregation and coring during solidification to study. The goal of selecting Al-Ag alloys was to study homogenization and the role of chemical inhomogeneity on solid-state phase transformations. As a model system, Al-Cu alloys were also selected to compare with previous rapid solidification studies and modeling [30.5] of microstructural evolution [30.1-30.2, 30.5-30.6].

30.3 Recent Progress

30.3.1 Rapid Solidification Studies at the Colorado School of Mines (CSM)

Preliminary rapid solidification studies were conducted at CSM using a laser welding set-up and Al-7 at.% Cu foil. The laser parameters for these experiments (100 IPM and 200 IPM for both 150 W and 200 W) were chosen based on the limits of the laser of a 200 W maximum power and 200 IPM maximum speed. The microstructures of these samples were examined in both the longitudinal and transverse directions of the welding pass, an example of which is given in **Figure 30.2**. Solidification speed was also calculated using the method shown in **Figure 30.3** [30.7], which calculates the velocity based on the equation:

$$V_s = V_b \cos(\theta) \qquad \text{Eqn. 30.1}$$

where V_s is the solidification velocity, V_b is the laser scan speed, and θ is the angle between the two vectors (**Figure 30.3**). Due to the inconsistent angle of the dendrites/cells growing in the longitudinal cross section, the angle measurement was taken in multiple places and averaged to find the solidification velocity. These results are given in **Table 30.2**, along with comparison values from the literature. As seen in the table, the calculated velocities were lower than typical rapid solidification values achieved via laser welding experiments. These experiments pushed the limits of the laser set up, creating a need for another technique to achieve higher solidification velocities. Melt spinning was identified as a viable method to reach higher solidification rates. Crucibles and samples are currently being prepared to run these experiments before the next reporting period.

30.3.2 DTEM of Al-Ge & Al-Ag

DTEM was performed in September 2018 to continue studies on Al-Ge and start imaging of Al-Ag alloys. The Ge-rich samples (i.e. measured to be > 58 at. %) with unverified compositions were analyzed to determine actual versus nominal compositions and the phases present. Similar to the two samples measured previously, which were targeted to have lower Ge contents of 33 and 40 at. % Ge, these samples exhibited higher Ge levels than the target values (**Table 30.2**). Phase identification is being performed on these samples and is still ongoing. Some preliminary results have been obtained on both the target 43 and 53 at. % Ge samples (measured to be 63 and 70-76 at. % Ge). These compositions contain large Ge-rich β phase crystals surrounded by eutectic, as expected from the phase diagram in **Figure 30.1**. These were seen to grown in a twinned fashion, and were surrounded by a eutectic that is still being identified. While the higher Ge sample (measured 70-76 at. %) shows just eutectic in between the β phase crystals**,** the lower Ge sample (measured 63 at. %) shows some Al rich dendrites and a small amount of eutectic between these crystals (**Figure 30.5**). This is most likely due to the local composition of the liquid in the melt after the Ge-rich crystals have formed. In the 63 at. % Ge sample, there is enough Ge taken from the liquid by the β phase crystals to generate a locally Al-rich region in the liquid, causing Al-rich dendrites to grow. In the 70-76 at. % Ge sample, there is still enough Ge locally in the liquid between the crystals to prevent these dendrites from growing, causing a eutectic to form. While the eutectic in the 70-76 at. % Ge sample is still being identified, the composition of the Al-rich (darker) and Ge-rich (lighter) areas of the 63 at. % Ge sample have been determined to be 22 at. % Ge and 78 at. % Ge, respectively. The M phase has been found in our previous work and that of others [30.8] to have a composition in a range of 43-45 at. % Ge. Other metastable phases that have been identified in this system fall between a range of 41-51 at. % Ge (**Table 30.3**) [30.8]. Because of this, it is likely that this eutectic is composed of two equilibrium phases, but more work needs to be done to confirm this hypothesis. It was also noticed that the Ge-rich phase in the eutectic appears to grow off of the Ge-rich crystals in this sample (**Figure 30.5**). This may correlate to a finding presented in [30.4], which observed that the metastable phases never grow with each other or with the β phase, but only form metastable equilibria with the α phase. This would imply that this eutectic is most likely α + β, as these would be the only two phases likely to grow off of the β phase crystal, as seen below. More work needs to

be done to confirm this hypothesis, however. Work is still underway to identify which phases are present in the eutectic, as well as to investigate the effects of local composition on the eutectic that forms. Alongside phase and composition studies, phase fractions will be determined to compare with the proposed metastable phase diagram by Laoui and Kaufman [30.4].

Recent DTEM experiments were designed to help fill in the gaps missed by our initial round of samples, due to target vs. measured composition variations. These samples were targeted at compositions closer to the 50.5 at. % Ge composition, especially on the Ge-rich side to capture the proposed re-melting of the M phase [30.4]. Initial Al-Ag compositions (targeted 10 and 30 at. % Ag) were also examined with DTEM during rapid solidification. Analysis of the collected data is underway.

30.3.2 Characterization of Aluminum MMC Powder

A more recent addition to this project proposes to study solidification of ceramic particle-containing aluminum alloy powder to understand the effect of inoculants on grain growth during rapid solidification. Initial characterization with scanning electron microscopy (SEM) of Al 6061 MMC powder is shown in **Figure 30.6**. These images were used to calculate particle sizes using ImageJ. The resulting size ranges are shown in **Table 30.4**, and were found to be on the order of tens of microns.

30.4 Plans for Next Reporting Period

Future work is currently focused on the analysis of recently and previously collected DTEM data, including includes phase identification and confirmation of compositions from the post-mortem samples, as well as image analysis of as-solidified microstructures. Melt spinning at CSM is also underway with crucible designs being tested. In 2019, in-situ imaging of metallic alloy rapid solidification will be performed at the Advanced Photon Source (APS) at Argonne National Laboratory with an additive manufacturing simulator (**Figure 30.7**) [30.3].

30.5 References

[30.1] J. Mckeown, K. Zweiacker, C. Liu, D. R. Coughlin, A. J. Clarke, J. K. Baldwin, J. W. Gibbs, J. D. Roehling, S. D. Imhoff, P. J. Gibbs, D. Tourret, J. M. K. Wiezorek, G. H. Campbell, Time-resolved in situ measurements during rapid alloy solidification: experimental insight for additive manufacturing, JOM, 68 (2016).

[30.2] J. Mckeown, A. Kulovits, C. Liu, K. Zweiacker, B. W. Reed, T. LaGrange, J. M. K. Wiezorek, G. H. Campbell, In situ transmission electron microscopy of crystal growth-mode transitions during rapid solidification of a hypoeutectic Al-Cu alloy, Acta Metallurgica et Materialia, 65 (2014) 56-68.

[30.3] C. Zhao, K. Fezzaa, R. Cunningham, H. Wen, F. De Carlo, L. Chen, A. D. Rollett, T. Sun, Real-time monitoring of laser powder bed fusion process using high-speed X-ray imaging and diffraction, Scientific Reports,7 (2017) 1-11, 2017.

[30.4] T. Laoui, M. Kaufman, Nonequilibrium behavior in the Al-Ge alloy system: insights into the metastable phase diagram, Metallurgical Transactions A, 22A (1991) 2141-2152.

[30.5] T. T. Roehling, S. S. Q. Wu, S. A. Khairallah, J. D. Roehling, S. S. Soezeri, M. F. Crumb, M. J. Matthews, Modeling laser intensity profile ellipticity for microstructural control during metal additive manufacturing, Acta Metallurgical et Materialia, 128 (2017) 197-206.

[30.6] D. Tourret, J. C. E. Mertens, E. Lieberman, S. D. Imhoff, J. W. Gibbs, K. Henderson, K. Fezzaa, A. L. Deriy, T. Sun, R. A. Lebensohn, B. M. Patterson, A. J. Clarke, From solidification processing to microstructure to mechanical properties: a multi-scale x-ray study of an Al-Cu alloy sample, Metallurgical and Materials Transactions A, 48A (2017) 5529-5546.

[30.7] J. D. Roehling, A. Perron, J. L. Fattebert, T. Haxhimali, G. Guss, T. T. Li, D. Bober, A. W. Stokes, A. J. Clarke, P. E. A. Turchi, M. J. Matthews, J. T. Mckeown, Rapid solidification in bulk Ti-Nb alloys by single-track laser melting, JOM, (2018) 1-9.

[30.8] M. Kaufman, J. Cunningham, H. Fraser, Metastable phase production and transformation in Al-Ge alloy films by rapid crystallization and annealing treatments, Acta Metallurgica et Materialia, 35 (1987) 1181-1192.

30.6 Figures and Tables

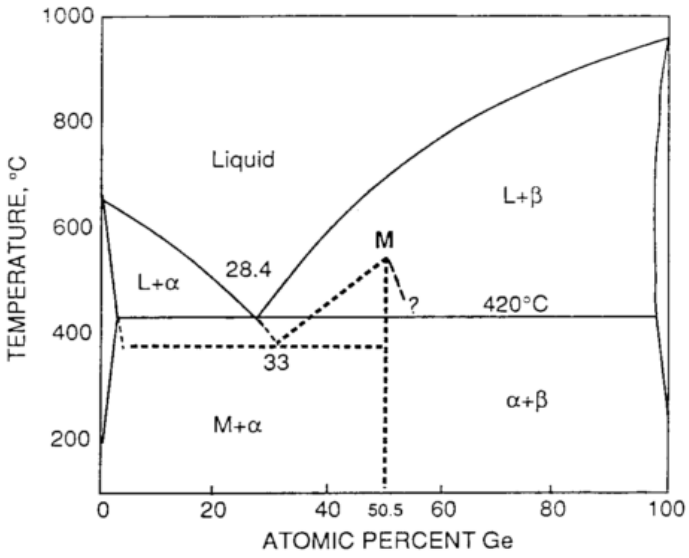

Figure 30.1: Al-Ge phase diagram, showing the proposed metastable phase diagram for the metastable monoclinic (M) phase [30.4].

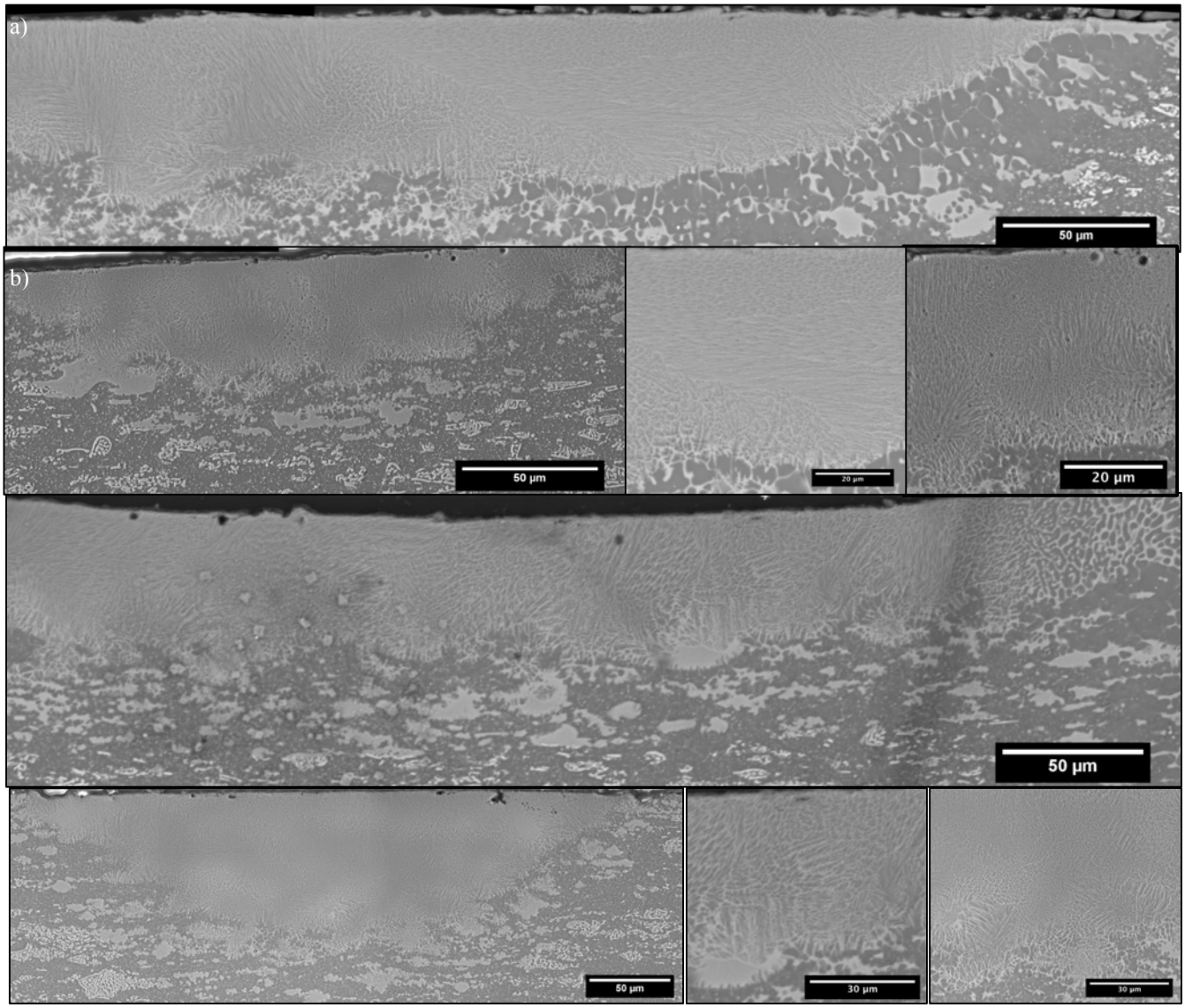

Figure 30.2: Microstructural results from laser welding of Al-7 at.% Cu for laser welding conditions of 150 W 200 IPM (a-d) and 200 W 200 IPM (e-h). The longitudinal cross-sections are shown in a) and e), the transverse in b) and f), and higher magnification images of both the longitudinal and transverse cross-sections are given by c) and g) and d) and h), respectively.

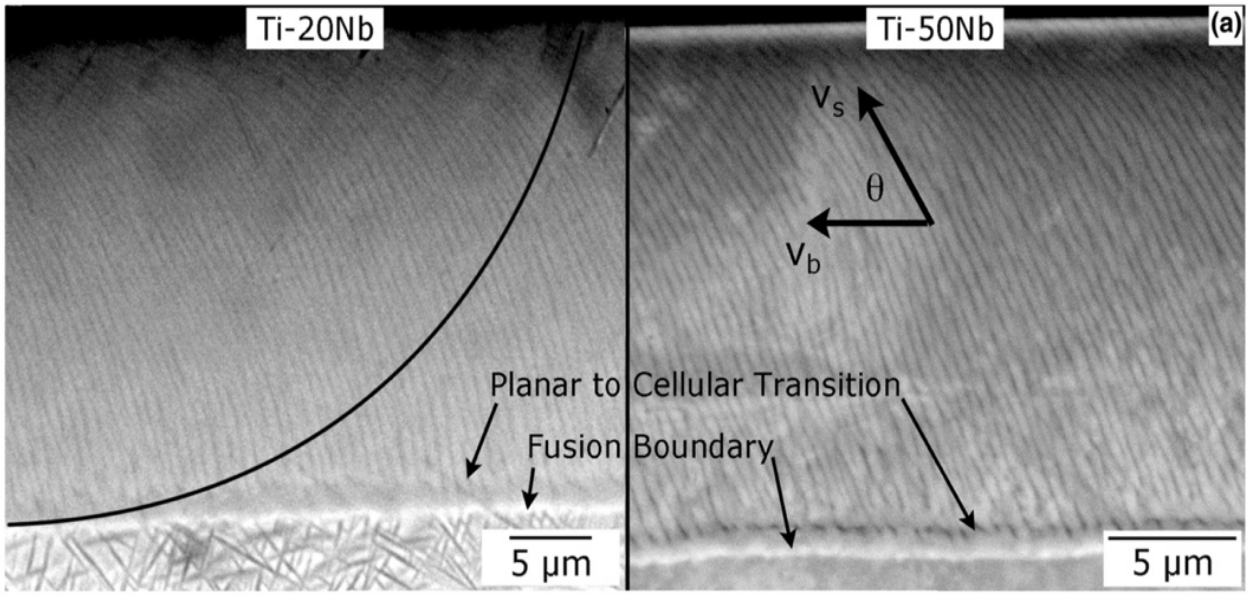

Figure 30.3: Images showing the method used to calculate solidification velocity for a laser welding experiment [30.10].

Table 30.1: Solidification Velocity of Laser Welds			
Welding Conditions	Average Solidification Velocity (mm/s)	Welding Conditions from Literature	Average Solidification Velocity from Literature (mm/s)
150 W, 42.3 mm/s	40.47	1200-1750 W, 100-4000 mm/s	200-600
150 W, 84.7 mm/s	53.16	1200-1750 W, 1-1000 mm/s	200-600
200 W, 42.3 mm/s	39.47		
200 W, 84.7 mm/s	45.82		

Table 30.2: Nominal and Measured Compositions of Al-Ge	
Nominal Composition (at. % Ge)	Measured Composition (at. % Ge)
33	46
40	58
43	63
53	70-76

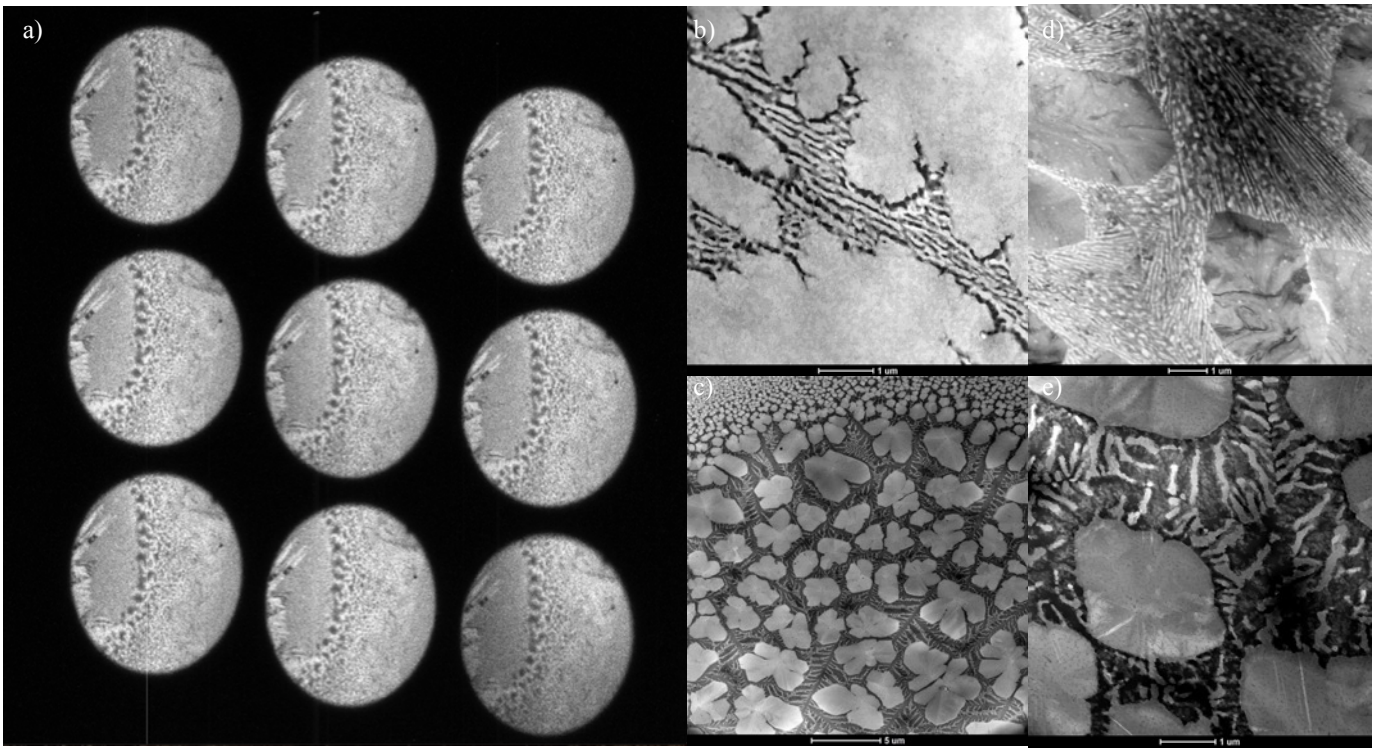

Figure 30.4: TEM micrographs of rapid solidified Al-Ge taken from DTEM samples. a) Dynamic data showing the M phase growing in from the left in the measured 46 at.% Ge sample. A post mortem image of these dendrites at higher magnification, surrounded by M + α eutectic, is shown in b). Post-mortem images of Ge-rich blocky β phase crystals in 58 at. %Ge, and two different morphologies of M + α eutectic in the same sample are shown in c), d), and e), respectively.

Table 30.3: Characteristics of Metastable Phases in Al-Ge

Phase (Space Group)	Lattice Parameter (nm)	Composition (at. % Ge)	Materials condition
M-phase ($P2_1/c$)	a = 0.673 b = 0.582 c = 0.805 β = 147.85°	43-45	Melt-spun ribbons Splat-quenched foils Submicron powders
R-phase (R-3c)	a = 0.767 α = 94.54°	49-51	Melt-spun ribbons Splat-quenched foils
O-phase (Pbca)	a = 0.78 b = 0.57 c = 0.73	41-50	Crystallized films
H-phase (P6/mmm)	a = 1.4 c = 0.72	42-45	Melt-spun ribbons Splat-quenched foils Submicron powders

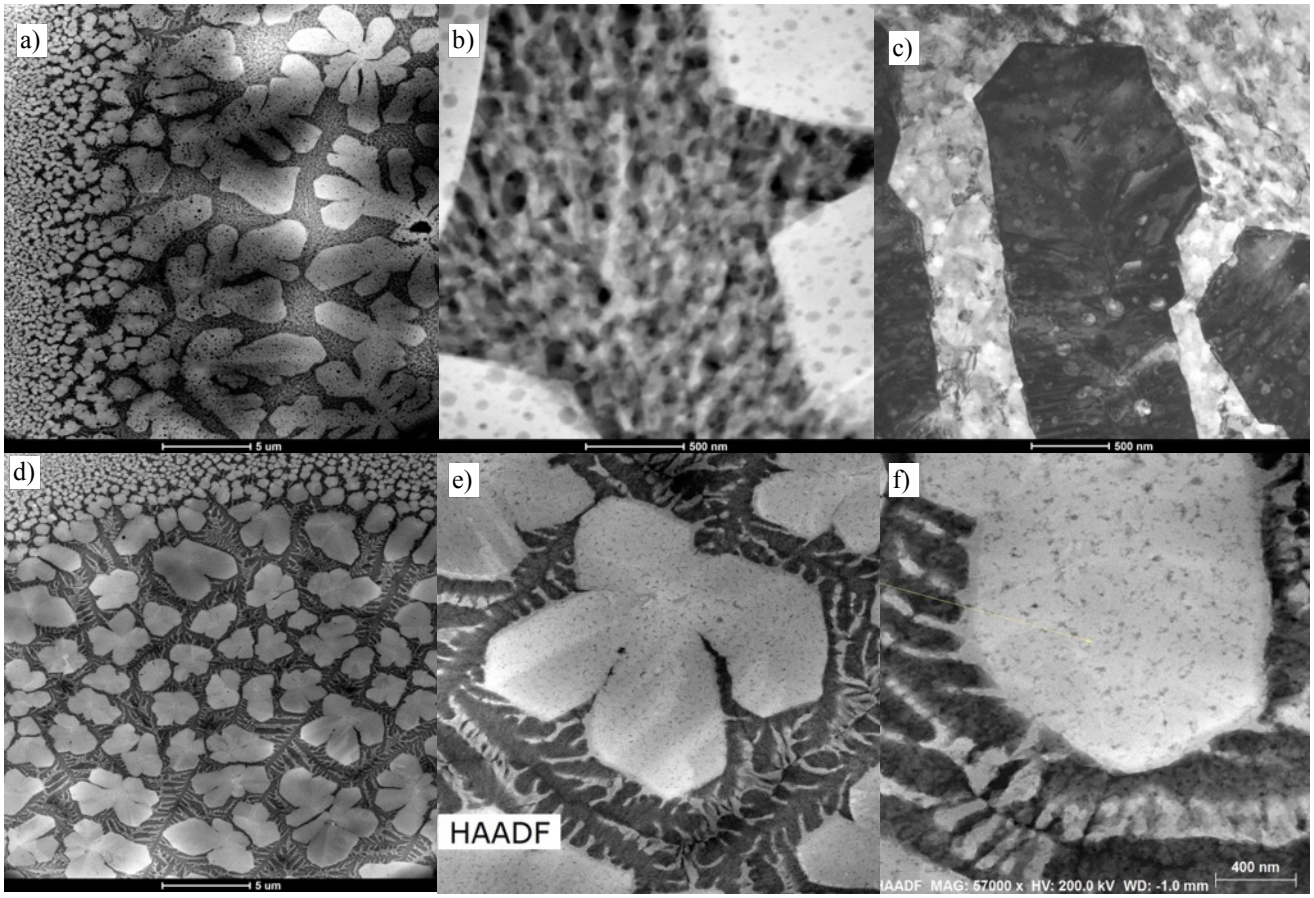

Figure 30.5: TEM micrographs of rapid solidified Al-Ge taken from DTEM samples. a) - c) show the measured 70-76 at. % Ge (targeted 53 at. % Ge) sample, whereas d) – e) show the measured 63 at. % Ge (targeted 43 at. % Ge). These show the large light-colored Ge-rich crystals surrounded by eutectic or Al- rich dendrites plus eutectic at the edge of a DTEM melt pool. a) & c) show the lower magnification HAADF images of the two samples, and b) & d) show higher magnification HAADF images of the eutectic (for b)) and the eutectic plus Al-rich dendrites (for d)) between the Ge-rich crystals. c) shows a BF image of a twinned arm of a Ge-rich crystal in the higher Ge composition, and f) shows the small layer of light colored phase in the eutectic that appears to grow off of the Ge-rich crystal.

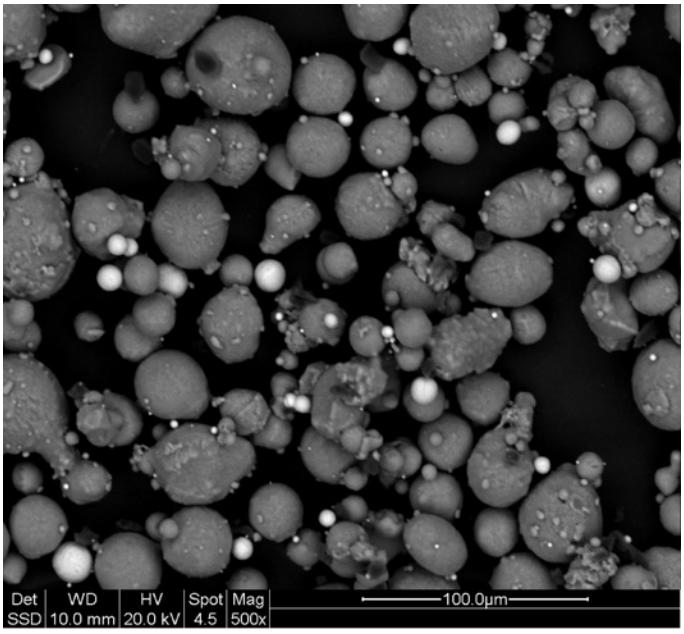

Table 30.4: Particle Size of Aluminum 6061 MMC Powder	
Range of Al6061 Particle Diameter (µm)	1-50
Total Average Particle Diameter (µm)	1.85
Range of Ceramic Particle Diameter (µm)	1-20
Ceramic Average Particle Diameter (µm)	5.10

Figure 30.6: SEM BSE image of Al 6061 alloy powder (grey) and ceramic particles (white).

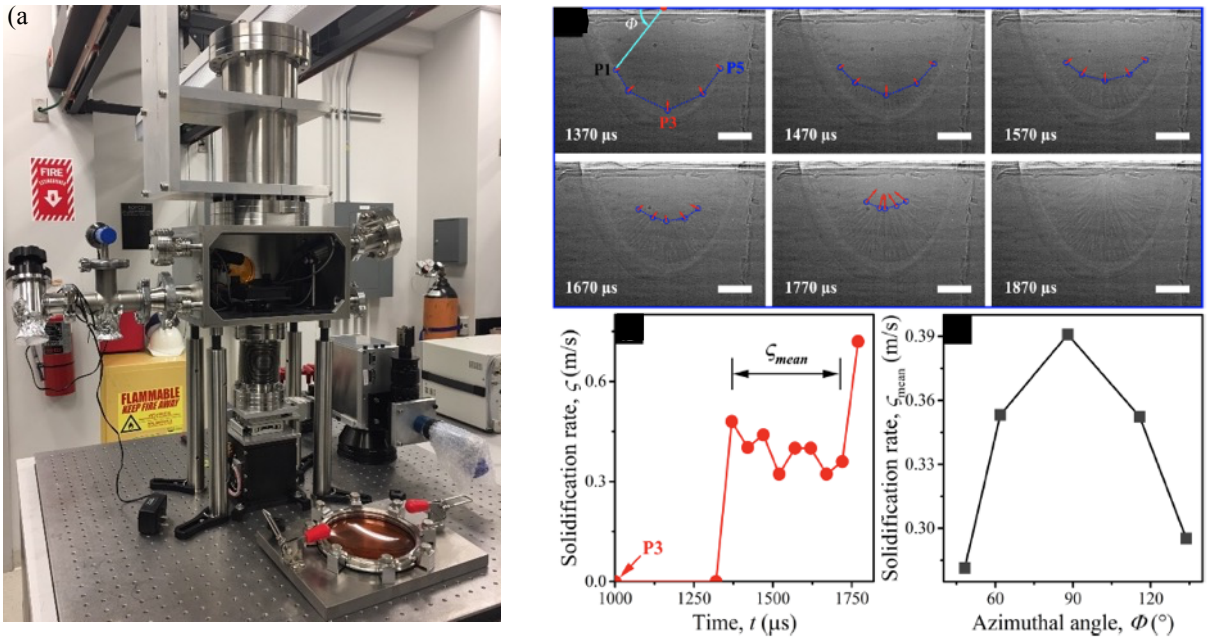

Figure 30.7: (a) Additive manufacturing set up at APS. (b) Imaging and solidification rate data taken from in-situ experiments [30.5].